Synthesis of the Two Isomers of Heteroleptic $Rh_{12}L_6L'_6$ Metal-Organic Polyhedra by Screening of Complementary Linkers

Anna Broto-Ribas,[a,b] María Susana Gutiérrez,[a,b] Inhar Imaz,[a,b,*] Arnau Carné-Sánchez,[a,b,*] Felipe Gándara,[c] Judith Juanhuix,[d] Daniel Maspoch,[a,b,e,*]

We have synthesised and characterised the two possible isomers of heteroleptic trigonal antiprismatic $M_{12}L_6L'_6$ MOPs by screening reactions of rhodium acetate with different pairs of complementary dicarboxylate linkers. The resulting 12 new MOPs (eight of isomer A + four of isomer B) are microporous in the solid state, exhibiting Brunauer-Emmett-Teller (BET) surface areas as high as 770 m^2/g.

Metal-organic polyhedra (MOPs) are nanoscale, zero-dimensional, discrete molecular cages comprising metal ions and clusters connected via organic linkers.[1,2] Owing to their molecular nature, they are soluble in various solvents, which facilitates their liquid processability, their use in the liquid phase for recognition and transport of molecules,[3,4] and stoichiometric control over their post-synthetic functionalisation.[5,6] Moreover, some MOPs are porous in the solid state, suggesting the synthesis of highly processable porous materials. However, the initial reports on the permanent porosity of MOPs have revealed only modest BET surface areas (S_{BET}), ranging from 10 m^2/g to 200 m^2/g. These low values have been attributed to the lack of structural stability of MOPs and to their lack of long-range order, which derives from their monomeric nature. However, researchers have recently reported much higher S_{BET} values, ranging from 600 m^2/g to 1300 m^2/g, for certain robust MOPs that contain strong carboxylate-metal ion bonds.[7,8] In particular, use of Zr(IV),[9] Mo(II),[10] Cr(II),[11] and Rh(II)[12] has provided access to new MOPs that are more porous and structurally more robust. Nevertheless, the reported MOPs that exhibit permanent porosity fall into three main geometric classes: cuboctahedra (most of which are analogous to the archetypical $Cu_{24}(bdc)_{24}$ structure),[1,2] octahedra,[13] or tetrahedra.[9] Less common geometries include cubes,[14] cigars,[15] lanterns,[16] triangular prisms,[17] icosahedra[18] and dodecahedra.[19]

One way to diversify the catalogue of permanently porous MOPs is to assemble new cages from at least two different linkers. Although this approach has been widely applied to Metal-Organic Frameworks (MOFs) and Covalent-Organic Frameworks (COFs),[20] it remains relatively unexplored for MOPs[21], as it requires that multiple linkers be carefully assembled into a single heteroleptic cage structure without concomitant formation of single-component homoleptic cages, mixtures of different multicomponent cages, and/or extended 2D or 3D networks. To face this challenge, researchers have proposed various synthetic methodologies, including the use of guest molecules as structure-directing agents or templates, and steric effects or shape-complementarity of ligands with different geometries.[22]

An example of the use of shape complementary ligands to form heteroleptic cages is the trigonal antiprismatic cages that are assembled from connecting six metal ions/paddlewheel clusters through six **L** linkers with a 60° bent angle and six **L'** linkers with a 120° bent angle (Fig. 1,top). These cages are composed of two trigonal macrocycles, each one built up from connecting three metal ions/clusters through three **L** or **L'** linkers. Both trigonal macrocycles, which form the top and bottom facets of the antiprism, are connected through the other six complementary linkers, which are in the equatorial positions of the antiprism. As the two types of linkers are in geometrically non-equivalent positions, two structural isomeric cages can be constructed (Fig. 1): Isomer A, in which the two trigonal macrocycles are assembled using **L'** linkers and then, both macrocycles are interconnected through **L** linkers;[23] and Isomer B, in which the positions of **L** and **L'** are inverted. Recently, both types of isomeric trigonal antiprismatic cages have been independently reported by groups that employed different coordination chemistries (Fig. 1, bottom). Thus, isomer A has been assembled by connecting Cu(II) paddlewheel clusters with two complementary dicarboxylate linkers.[24–27] Alternatively, isomer B has been synthesised by the assembly of Pd(II) ions with two complementary linkers based on pyridine moieties.[28]

Herein we endeavoured to form such trigonal antiprismatic cages using paddlewheel Rh(II) clusters, which have been demonstrated to form strong carboxylate-metal ion bonds that lead to the formation of structurally robust and porous MOPs. To this end, we crossed two dicarboxylate linkers ($\mathbf{L^1}$ & $\mathbf{L^2}$) with six other dicarboxylate linkers ($\mathbf{L^{1\text{-}6'}}$) to synthesize twelve different trigonal antiprismatic $Rh_{12}\mathbf{L}_6\mathbf{L'}_6$ MOPs (Fig. 2). We found that, analogously to previously reported Cu(II) paddlewheel-based trigonal antiprismatic cages (Fig. 1,bottom), the most abundant $Rh_{12}\mathbf{L}_6\mathbf{L'}_6$ cage was isomer A. However, we also found that, depending on the combination of complementary linkers, the relative position of both **L** and **L'** can be exchanged to give rise to isomer B. To our knowledge, this isomer has not previously been reported for metal-carboxylate

[a.] *Catalan Institute of Nanoscience and Nanotechnology (ICN2), CSIC and The Barcelona Institute of Science and Technology, Campus UAB, 08193 Bellaterra, Barcelona, Spain*
[b.] *Departament de Química, Facultat de Ciències, Universitat Autònoma de Barcelona, 08193, Bellaterra, Spain*
[c.] *Department of New Architectures in Materials Chemistry, Materials Science Institute of Madrid – CSIC, Sor Juana Inés de la Cruz 3, 28049 Madrid, Spain*
[d.] *ALBA Synchrotron, 08290 Cerdanyola del Vallès, Barcelona, Spain*
[e.] *ICREA, Pg. Lluís Companys 23, 08010 Barcelona, Spain*
† Footnotes relating to the title and/or authors should appear here.
Electronic Supplementary Information (ESI) available: [details of any supplementary information available should be included here]. See DOI: 10.1039/x0xx00000x

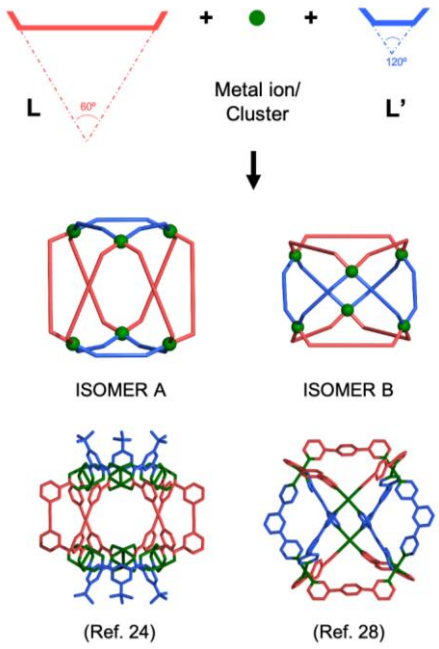

Figure 1. Schematic of the formation of the two possible structural isomers of the trigonal antiprismatic cages assembled from a metal ion/cluster and a pair of complementary linkers, denoted in each case as **L** and **L'**. Bottom: crystal structures of the first-ever reported, trigonal antiprismatic cages, isomers A & B. Isomer A was built up by connecting Cu(II) paddlewheels through 3,3'-(ethyne-1,2-diyl)dibenzoic acid as **L**, and 5-*tert*-butylbenzene-1,3-dicarboxylic acid, as **L'**. Isomer B was built up by connecting Pd(II) ions through 3,3'-(1,4-phenylene)dipyridine as **L**, and 4,4'-(1,3-phenylene)dipyridine as **L'**.

cages. For these $Rh_{12}L_6L'_6$ MOPs, we measured nitrogen Brunauer-Emmett-Teller surface areas (S_{BET}) as high as 776 m^2/g, thus confirming their porosity in the solid-state.

We began by mixing rhodium acetate with the linker $\mathbf{L^1}$ and, independently, each of the five complementary derivatives of the BDC linker $\mathbf{L^{1\text{-}5'}}$. Thus, we reacted the two linkers, $\mathbf{L^1}$ and one of $\mathbf{L^{1\text{-}5'}}$, with rhodium acetate under solvothermal conditions in dimethylacetamide (DMA) in the presence of Na_2CO_3 at 100 °C for 72 h. All these reactions yielded brownish-green solutions, which were centrifuged to facilitate removal of the Na_2CO_3. Each supernatant was added dropwise to cold MeOH, which induced the precipitation of green powders, each of which was isolated by centrifugation. Spectroscopic characterisation was consistent with formation of the expected heteroleptic MOPs of formula $Rh_{12}\mathbf{L^1}_6\mathbf{L^{1\text{-}5'}}_6$. Specifically, analysis of the ^{1}H-NMR spectra of digested $Rh_{12}\mathbf{L^1}_6\mathbf{L^{1\text{-}5'}}_6$ confirmed the expected 1:1 ratio between $\mathbf{L^1}$ and each of $\mathbf{L^{1\text{-}5'}}$ (Fig. S6-10). Moreover, the UV-vis spectra of $Rh_{12}\mathbf{L^1}_6\mathbf{L^{1\text{-}5'}}_6$ showed the characteristic band centred at 589-593 nm, which we ascribed to the $\pi^* \rightarrow \sigma^*$ transition of Rh(II) paddlewheel clusters (λ_{max}) (Fig. S18, S20, S22, S24, S26). Finally, the MALDI-TOF spectra contained a peak that evidences the expected molecular mass for the MOPs made from the assembly of six paddlewheel Rh(II) clusters, six $\mathbf{L^1}$ and six linkers $\mathbf{L^{1\text{-}5'}}$, of formula $[Rh_{12}(\mathbf{L^1})_6(\mathbf{L^{1'}})_6 + H]^+$ (m/z = 3817.9 g/mol); $[Rh_{12}(\mathbf{L^1})_6(\mathbf{L^{2'}})_6(DMA)(H_2O)_2(MeOH)_4 + H]^+$ (m/z = 4405.3 g/mol); $[(Rh_6(\mathbf{L^1})_6(\mathbf{L^{3'}})_6(DMA)_2(H_2O)_2(MeOH)+H]^+$(m/z = 4491.7 g/mol); $[Rh_{12}(\mathbf{L^1})_6(\mathbf{L^{4'}})_6(DMA)_2(H_2O)_4 + H]^+$ (m/z = 4669.6 g/mol); $[(Rh_6(\mathbf{L^1})_6(\mathbf{L^{5'}})_6) + H]^+$ (m/z = 4925.1 g/mol) (Fig. S35-S39).

Having acquired a convincing body of spectroscopic evidence to corroborate the formation of heteroleptic $Rh_{12}\mathbf{L^1}_6\mathbf{L^{1\text{-}5'}}_6$, we next determined their isomeric structure through Single-Crystal X-ray Diffraction (SCXRD). Note that, for the formation of single crystals suitable for SCXRD, $Rh_{12}\mathbf{L^1}_6\mathbf{L^{1\text{-}5'}}_6$ were all crystallised by first pre-coordinating a functionalised pyridine to the Rh(II) sites of the polyhedral cage. Accordingly, a DMA or DMF solution of 4-hydroxypyridine or isonicotinic acid was added to a solution of $Rh_{12}\mathbf{L^1}_6\mathbf{L^{1\text{-}5'}}_6$ in either DMA or a mixture of DMA/DMF. Immediately afterwards, all the green suspensions of $Rh_{12}\mathbf{L^1}_6\mathbf{L^{1\text{-}5'}}_6$ became purple solutions. The UV-Vis spectra of these solutions revealed a λ_{max} centred at 552-559 nm, which corresponds to one 4-hydroxypyridine or isonicotinic acid ligand coordinated to one Rh(II) paddlewheel through its axial site (Fig. S19, S21, S23, S25, S27).[5] Single purple parallelepiped crystals of $Rh_{12}\mathbf{L^1}_6\mathbf{L^{1'}}_6$ and of $Rh_{12}\mathbf{L^1}_6\mathbf{L^{3'}}_6$, and cubic crystals of $Rh_{12}\mathbf{L^1}_6\mathbf{L^{4'}}_6$ and of $Rh_{12}\mathbf{L^1}_6\mathbf{L^{5'}}_6$, were obtained by slow diffusion of ether vapours into the DMA or DMA/DMF solutions. SCXRD data revealed the formation of heteroleptic, trigonal, antiprismatic $Rh_{12}\mathbf{L}_6\mathbf{L'}_6$ MOPs having the structure of isomer A (Fig. 2). In these cages, the top and bottom trigonal facets (aperture diameter: 3.8 Å) are formed by the connection of three paddle-wheel Rh(II) clusters through three $\mathbf{L^{1\text{-}5'}}$ linkers. These two triangular facets are connected by six $\mathbf{L^1}$ linkers to form six larger triangular windows (aperture diameter: 6.6 Å), which are delineated by two $\mathbf{L^1}$ linkers and one $\mathbf{L^{1\text{-}5'}}$ linker. In these isostructural cages, the functional groups placed in the isophthalate-based linker **L'** define the functionalisation of the top and bottom triangular facets of the antiprism (Fig. 2). For all these MOPs, experimental Powder X-ray Diffraction (PXRD) patterns matched the corresponding simulated patterns from the crystal structures (Fig. S47-S51), thereby confirming their phase purity.

Next, we studied the influence of the length of **L'** on formation of the cage. To this end, we used the naphthalene-based linker $\mathbf{L^{6'}}$, which contains one more phenyl ring than do the linkers $\mathbf{L^{1\text{-}5'}}$. Reaction of $Rh_2(acetate)_4$ with the linkers $\mathbf{L^1}$ and $\mathbf{L^{6'}}$, and Na_2CO_3 in DMA under similar solvothermal conditions

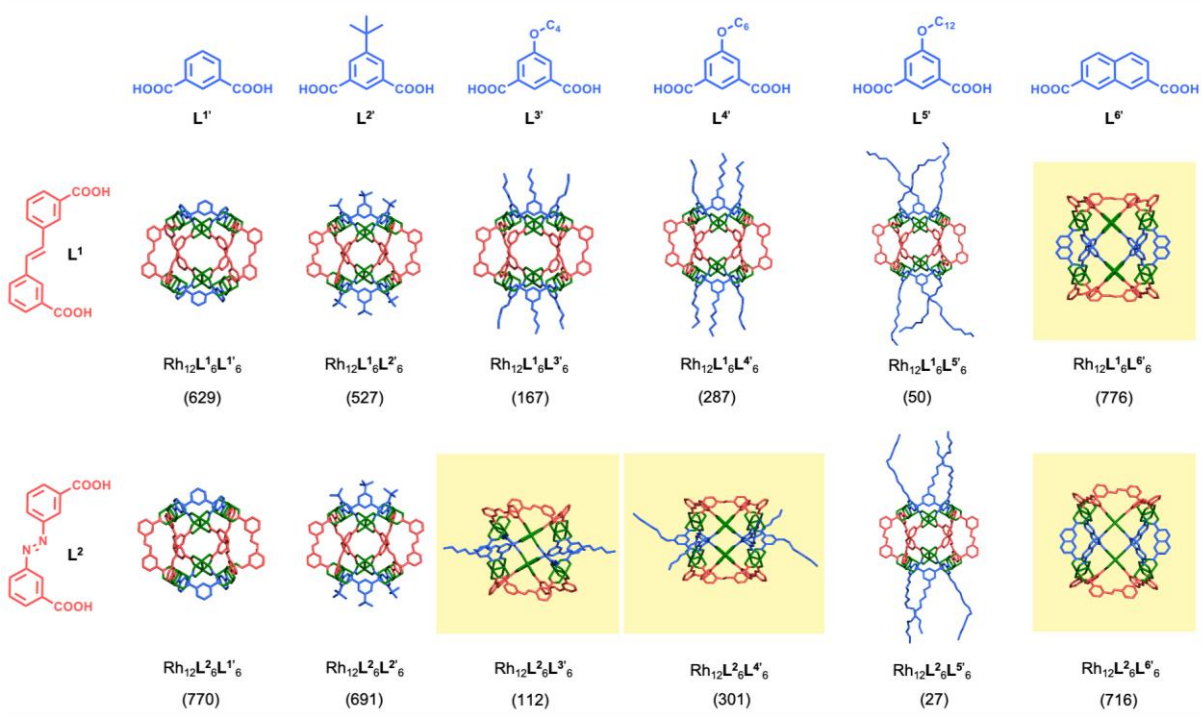

Figure 2. Representation of the complementary linkers $\mathbf{L^{1\text{-}2}}$ and $\mathbf{L^{1\text{-}6\prime}}$, and the crystal structures of the corresponding isomeric trigonal antiprismatic cages assembled with Rh(II), as either isomer A (white background) or isomer B (yellow boxes). The corresponding S_{BET} values (in m^2/g) are shown below each formula.

produced a green powder, which we identified as the expected heteroleptic $Rh_{12}\mathbf{L^1}_6\mathbf{L^{6\prime}}_6$ MOP by ^{1}H-NMR, UV-Vis, and MALDI-TOF (Fig. S11, S28, S40). Single-crystals suitable for SCXRD were obtained by dissolving the powder in DMF in the presence of isonicotinic acid, and then exposing the resulting solution to ether vapours. Unexpectedly, SCXRD data revealed the formation of the trigonal antiprismatic MOP exhibiting the structure of isomer B (Fig. 2 and 3). In it, the top and bottom trigonal facets (aperture diameter: 8.6 Å) are formed by the connection of three paddlewheel Rh(II) clusters through three $\mathbf{L^1}$ linkers. These two trigonal facets are connected by six $\mathbf{L^{6\prime}}$ linkers, thereby forming six larger triangular windows (aperture diameter: 6.6 Å) that are delineated by two naphthalene moieties and one $\mathbf{L^1}$ linker. The experimental XRPD pattern of these $Rh_{12}\mathbf{L^1}_6\mathbf{L^{6\prime}}_6$ crystals matched the simulated pattern from the crystal structure, thus confirming its phase purity (Fig. S52).

Having observed that both isomeric trigonal antiprismatic MOPs could be assembled depending on the complementary dicarboxylate linkers, we sought to validate our observations by creating six additional heteroleptic MOPs combining $\mathbf{L^{1\text{-}6\prime}}$ with $\mathbf{L^2}$, which contains an azo group in place of the olefinic group in $\mathbf{L^1}$ (Fig. 2). We began by mixing rhodium acetate with $\mathbf{L^2}$ and the naphthalene-based $\mathbf{L^{6\prime}}$, from which isomer B was again assembled. We then combined rhodium acetate with $\mathbf{L^2}$ and the other, isophthalate-based, $\mathbf{L^{1\text{-}5\prime}}$. These reactions led to formation of either isomer A, when $\mathbf{L^2}$ was combined $\mathbf{L^{1\prime}}$, $\mathbf{L^{2\prime}}$ and $\mathbf{L^{5\prime}}$, or isomer B, when $\mathbf{L^2}$ was combined with $\mathbf{L^{3\prime}}$ or $\mathbf{L^{4\prime}}$. Altogether, our results suggest that both isomers of trigonal antiprismatic MOPs are accessible, and that minor variations in the length and functionalities of the complementary linkers can tip the balance in favour of one isomer or the other.

Once we had synthesised the library of 12 new, heteroleptic, trigonal antiprismatic Rh-MOPs, we assessed their solid-state porosity by subjecting them to N_2 adsorption experiments at 77 K (Fig. S59-70). All $Rh_{12}\mathbf{L}_6\mathbf{L'}_6$ MOPs were microporous in the solid state, as evidenced by their corresponding type I isotherms, from which we determined the corresponding S_{BET} values (Fig. 2). Remarkably, these values further support the premise that use of Rh(II) ions tends to form stable and highly porous MOPs in the solid state, whereby steric hindrance around the MOP core remains the principal hurdle to porosity, as commonly observed in archetypical cuboctahedral Rh(II) MOPs.[5] Accordingly, regardless of the isomer, the four heteroleptic MOPs assembled by combining either $\mathbf{L^1}$ or $\mathbf{L^2}$ with either $\mathbf{L^{1\prime}}$ or $\mathbf{L^{6\prime}}$ exhibited the highest S_{BET} values (range: 696 to 770 m^2/g) (Fig. 3b). Similarly, the two heteroleptic MOPs built up either from $\mathbf{L^1}$ or $\mathbf{L^2}$ with (the *tert*-butyl-functionalised) $\mathbf{L^{2\prime}}$ exhibited S_{BET} values of 528 and 686 m^2/g, respectively. Finally, encouraged by the robustness, porosity and accessible metal sites of our heteroleptic Rh(II) MOPs, we also evaluated their capacity for CO_2 adsorption at 298 K (Fig. 3c, S71-82), observing CO_2 uptake values from 2.56 to 10.95 mol CO_2/ mol MOP.

To conclude, we have synthesised and characterised a family of 12, new, heteroleptic, trigonal antiprismatic porous MOPs. We discovered that, depending on the combination of complementary linkers, the two possible heteroleptic cage isomers could be assembled. We have also demonstrated that the external functionality of these MOPs can be tailored by means of isoreticular chemistry. Moreover, all these MOPs are microporous in the solid state, enlarging the still short-list of porous cages.

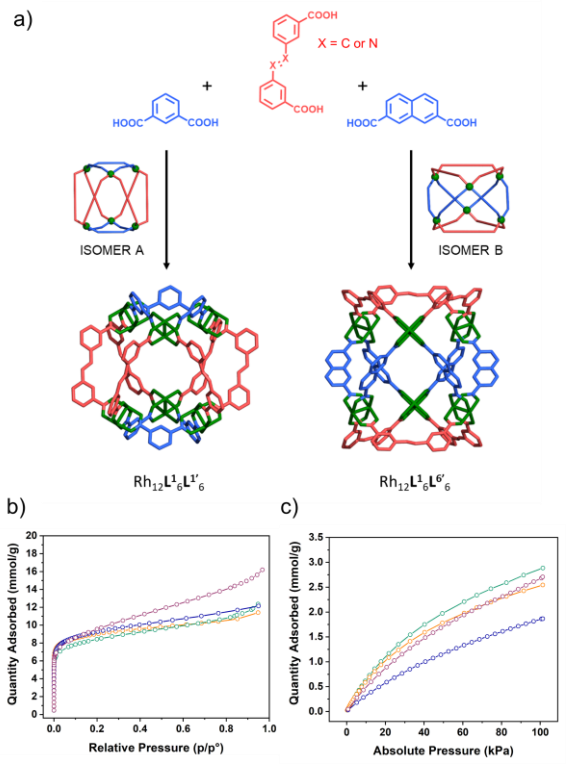

Figure 3. a) Schematic of the formation of both isomers, A and B, upon changing the length of linker **L'**. b,c) N_2 (b) and CO_2 (c) sorption isotherm for $Rh_{12}L_6L'^1{}_6$ (green), $Rh_{12}L^2{}_6L'^1{}_6$ (orange), $Rh_{12}L_6L'^5{}_6$ (red) and $Rh_{12}L^2{}_6L'^5{}_6$ (blue).

This work was supported by Spanish MINECO (project RTI2018-095622-B-I00) and "la Caixa" Foundation (ID 100010434; fellowship: LCF/BQ/PR20/ 11770011). ICN2 is supported by the Severo Ochoa programme from Spanish MINECO (Grant No. SEV-2017-0706).

Conflicts of interest

There are no conflicts to declare.

Notes and references

1 M. Eddaoudi, J. Kim, J. B. Wachter, H. K. Chae, M. O'Keeffe and O. M. Yaghi, *J. Am. Chem. Soc.*, 2001, **123**, 4368–4369.

2 B. Moulton, J. Lu, A. Mondal and M. J. Zaworotko, *Chem. Commun.*, 2001, **2**, 863–864.

3 L. Hernández-López, J. Martínez-Esaín, A. Carné-Sánchez, T. Grancha, J. Faraudo and D. Maspoch, *Angew. Chem. Int. Ed.*, 2021, **60**, 11406–11413.

4 T. Grancha, A. Carné-Sánchez, L. Hernández-López, J. Albalad, I. Imaz, J. Juanhuix and D. Maspoch, *J. Am. Chem. Soc.*, 2019, **141**, 18349–18355.

5 A. Carné-Sánchez, J. Albalad, T. Grancha, I. Imaz, J. Juanhuix, P. Larpent, S. Furukawa and D. Maspoch, *J. Am. Chem. Soc.*, 2019, **141**, 4094–4102.

6 G. Liu, Y. Di Yuan, J. Wang, Y. Cheng, S. B. Peh, Y. Wang, Y. Qian, J. Dong, D. Yuan and D. Zhao, *J. Am. Chem. Soc.*, 2018, **140**, 6231–6234.

7 S. Lee, H. Jeong, D. Nam, M. S. Lah and W. Choe, *Chem. Soc. Rev.*, 2021, **50**, 528–555.

8 E. J. Gosselin, C. A. Rowland and E. D. Bloch, *Chem. Rev.*, 2020, **120**, 8987–9014.

9 G. Liu, Z. Ju, D. Yuan and M. Hong, *Inorg. Chem.*, 2013, **52**, 13815–13817.

10 J. R. Li, A. A. Yakovenko, W. Lu, D. J. Timmons, W. Zhuang, D. Yuan and H. C. Zhou, *J. Am. Chem. Soc.*, 2010, **132**, 17599–17610.

11 J. Park, Z. Perry, Y. P. Chen, J. Bae and H. C. Zhou, *ACS Appl. Mater. Interfaces*, 2017, **9**, 28064–28068.

12 S. Furukawa, N. Horike, M. Kondo, Y. Hijikata, A. Carné-Sánchez, P. Larpent, N. Louvain, S. Diring, H. Sato, R. Matsuda, R. Kawano and S. Kitagawa, *Inorg. Chem.*, 2016, **55**, 10843–10846.

13 Z. Ni, A. Yassar, T. Antoun and O. M. Yaghi, *J. Am. Chem. Soc.*, 2005, **127**, 12752–12753.

14 Z. Ju, G. Liu, Y. S. Chen, D. Yuan and B. Chen, *Chem. - A Eur. J.*, 2017, **23**, 4774–4777.

15 L. J. Cheng, X. X. Fan, Y. P. Li, Q. H. Wei, F. R. Dai, Z. N. Chen and Z. Wang, *Inorg. Chem. Commun.*, 2017, **78**, 61–64.

16 G. A. Craig, P. Larpent, S. Kusaka, R. Matsuda, S. Kitagawa and S. Furukawa, *Chem. Sci.*, 2018, **9**, 6463–6469.

17 K. Su, F. Jiang, J. Qian, L. Chen, J. Pang, S. M. Bawaked, M. Mokhtar, S. A. Al-Thabaiti and M. Hong, *Inorg. Chem.*, 2015, **54**, 3183–3188.

18 D. Geng, X. Han, Y. Bi, Y. Qin, Q. Li, L. Huang, K. Zhou, L. Song and Z. Zheng, *Chem. Sci.*, 2018, **9**, 8535–8541.

19 Z. Lu, C. B. Knobler, H. Furukawa, B. Wang, G. Liu and O. M. Yaghi, *J. Am. Chem. Soc.*, 2009, **131**, 12532–12533.

20 H. Furukawa, U. Müller and O. M. Yaghi, *Angew. Chem. Int. Ed.*, 2015, **54**, 3417–3430.

21 S. Pullen and G. H. Clever, *Acc. Chem. Res.*, 2018, **51**, 3052–3064.

22 S. Pullen, J. Tessarolo and G. H. Clever, *Chem. Sci.*, 2021, **12**, 7269–7293.

23 Y. Yang, A. Broto-Ribas, B. Ortín-Rubio, I. Imaz, F. Gándara, A. Carné-Sánchez, V. Guillerm, S. Jurado, F. Busqué, J. Juanhuix and D. Maspoch, *Angew. Chemie Int. Ed.*, 2022, **61**, e202111228.

24 J. R. Li and H. C. Zhou, *Nat. Chem.*, 2010, **2**, 893–898.

25 N. Hosono, K. Omoto and S. Kitagawa, *Chem. Commun.*, 2017, **53**, 8180–8183.

26 M. Do, D. Rogers, W. Kaminsky and D. J. Xiao, *Inorg. Chem.*, 2021, **60**, 7602–7606.

27 K. Omoto, N. Hosono, M. Gochomori, K. Albrecht, K. Yamamoto and S. Kitagawa, *Chem. Commun.*, 2018, **54**, 5209–5212.

28 S. Sudan, R. J. Li, S. M. Jansze, A. Platzek, R. Rudolf, G. H. Clever, F. Fadaei-Tirani, R. Scopelliti and K. Severin, *J. Am. Chem. Soc.*, 2021, **143**, 1773–1778.